Characterizing Transition-Challenging Regions Leveraging the Elliptic Restricted Three-Body Problem: L_2 Halo Orbits

Beom Park* and Kathleen C. Howell†
Purdue University, West Lafayette, IN, 47907

Structures in the Circular Restricted Three-Body Problem (CR3BP) are vital to enable multiple space mission concepts, yet delivering their counterparts in a Higher-Fidelity Ephemeris Model (HFEM) poses a non-trivial task. Achieving a seamless transition between the CR3BP and HFEM necessitates a thorough comprehension of the underlying dynamical factors that impede the process. This investigation leverages the Elliptic Restricted Three-Body Problem (ER3BP) as an intermediate model between the CR3BP and HFEM, employing numerical continuation and bifurcation analysis to characterize the challenges associated with the transition process. Specifically, the focus is on the Earth-Moon L_2 halo orbit family. A subset of the family exhibits a proliferation of fold bifurcations with respect to the eccentricity of the model, serving as an indicator for transition-challenging behavior as analyzed within the ER3BP.

I. Introduction

Structures that exist within the context of Circular Restricted Three-Body Problem (CR3BP) are pivotal for supporting a variety of space mission concepts. Such structures include periodic and quasi-periodic orbits that offer trajectories with desired stability characteristics, enabling efficient and strategic long-term presence throughout space. Within the Earth-Moon system, a prominent illustration is the 9:2 Near Rectilinear Halo Orbit (NRHO), known for its near-stability and access to the lunar vicinity [1]. It has been designated as the baseline orbit for the Gateway mission, aimed at reestablishing a sustainable human presence in cislunar space [2]. Similarly, in the context of the Sun-Earth system, NASA's Interstellar Mapping and Acceleration Probe (IMAP) [3] and the James Webb Space Telescope (JWST) [4] missions leverage Sun-Earth L_1 and L_2 libration point orbits, respectively.

The structures supplied by the CR3BP framework necessitate the *transition* into a Higher-Fidelity Ephemeris Model (HFEM) suitable for flight, while preserving the desirable characteristics obtained within the CR3BP. This transitioning process often entails the use of a differential corrections scheme, with the CR3BP trajectories serving as suitable initial guesses. Dei Tos [5] emphasizes the non-trivial aspect of this process, where the number of constraints is less than the number of free variables typically due to the loss of periodicity within the HFEM. The underconstrained nature of the problem renders it non-trivial and is somewhat arbitrary to define and compute suitable counterparts within the HFEM. Various methods exist to supply the search direction for the corrector, with the minimum-norm Newton-Raphson method [1, 6, 7] being commonly utilized to construct trajectories that closely align with the original geometry obtained from the CR3BP. Optimizers are also employed to control the properties of the converged solutions within the HFEM [8]. Other factors such as the transition epoch, number of segments, and rotation schemes all influence the solutions produced in the HFEM.

While experimenting with the specifics of the numerical transition scheme may deliver desired solutions, scenarios exist where the CR3BP initial guesses do not supply an adequate initial guess due to underlying dynamical factors. In such cases, it is possible that the HFEM solution basin deviates significantly from the CR3BP solution or even ceases to exist. One potential example for this *transition-challenging* behavior exists in the Earth-Moon L_2 halo family. Multiple authors [6, 9, 10] observe that a subset of the family near the $3:1$ synodic resonance period ratio exhibits more randomness when transitioned into the HFEM counterparts. For this region, producing the ballistic long-term ephemeris analogs solely relying on the CR3BP orbit as an initial guess is challenging [11]. Figure 1 illustrates such behavior, where utilizing the CR3BP orbits as the initial guess for a differential corrector results in significantly shorter horizon times for a subset of the Earth-Moon L_2 halo family, corresponding to a range from 8.6 to 11.0 days for the periods of the CR3BP halo orbits.

The current research investigation aims to identify the intrinsic dynamical factors contributing to the challenges encountered in transitioning CR3BP structures into the HFEM, with a specific focus on the Earth-Moon L_2 halo family.

*Ph.D. Candidate, School of Aeronautics and Astronautics, Purdue University, park1103@purdu.edu, AIAA Student Member
†Hsu Lo Distinguished Professor of Aeronautics and Astronautics, School of Aeronautics and Astronautics, Purdue University, AIAA Fellow

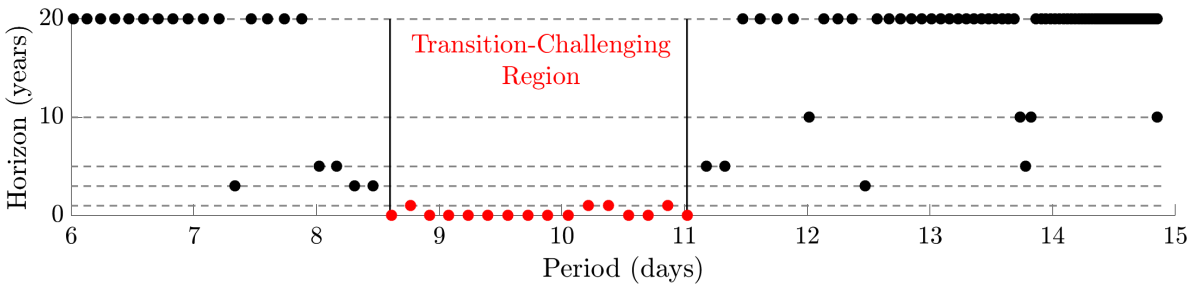

Fig. 1 ***Transition-challenging*** **region within the Earth-Moon L_2 halo family, recreated from Park and Howell, Figure 2. [11]**

This understanding is critical for several reasons. Examining regions posing transition challenges is expected to yield insights into the evolution and potential destruction of HFEM solutions that originate from CR3BP structures. This understanding aids in identifying regions where transitioning CR3BP structures is inherently challenging, without the need for extensive numerical transition investigations that are subject to multiple variables. Moreover, identifying the dynamical causes for transition challenges renders the foundation for an updated, alternative numerical transition scheme that accommodates HFEM solutions even when the CR3BP orbit geometry does not serve as a suitable initial guess. This adaptability offers the potential for versatile utilization of orbit structures tailored for various future space missions. With the Earth-Moon L_2 halo family as an example, the transition-challenging subset includes a $3:1$ synodic resonant orbit that provides a desirable linear stability and eclipse properties within the CR3BP, serving as candidate destinations for various objectives [6]. Identifying the underlying dynamical factors for the transition challenges is a necessary step in developing potential mitigation strategies to leverage these CR3BP structures. Given this significance, the current study serves as an initial survey showcasing the causes underlying transition challenges, with a specific focus on the challenging regions within the Earth-Moon L_2 halo family.

The current work leverages an intermediate model between the CR3BP and HFEM, specifically the Elliptic Restricted Three-Body Problem (ER3BP), for an efficient characterization of the transition-challenging behavior. Boudad and Howell [9] reveal that analysis within the CR3BP alone, such as stability and bifurcation analysis, does not provide sufficient insight into the perturbations that exist in the HFEM or the evolution of CR3BP solutions under the HFEM dynamics. Conversely, direct analysis within the HFEM can be overly complex. Previous investigations suggest that the Sun-Earth-Moon HFEM involves at least five distinct frequencies [12, 13]. Thus, it is impractical to characterize the underlying dynamical causes for transition behaviors simultaneously under multiple frequencies. Therefore, employing intermediate models that integrate perturbations in ideal forms associated with a single frequency presents a practical alternative. Periodically perturbed Hamiltonian systems of this nature enable analysis of the evolution of CR3BP structures through numerical continuation and bifurcation analysis. Park and Howell [10, 11] observe that the most significant source of perturbation within the Earth-Moon L_2 halo family in the HFEM is the time-varying distance between Earth and the Moon (pulsation). The Earth-Moon ER3BP interjects realistic pulsation magnitude and appropriate frequency information, serving as a suitable intermediate model that approximates the most impactful time-dependent perturbations within the HFEM during the transition of Earth-Moon L_2 halo orbits. It is important to note that various periodically perturbed models exist to represent the pulsation of the Earth-Moon system, each providing valuable insights. For instance, refer to Sanaga and Howell [14, 15] as well as Henry et al. [16] for illustrative examples that leverage the Hill Restricted Four-Body Problem as an alternative.

This investigation concentrates on the transformation of CR3BP halo periodic orbits into their ER3BP counterparts, manifesting as either periodic or quasi-periodic orbits. Employing numerical continuation schemes, bifurcation analyses within the ER3BP are examined to identify regions where transitions from the CR3BP to HFEM are *expected* to pose challenges. Specifically, the paper suggests the existence of fold bifurcations as a viable metric to characterize the transition challenges. The subsequent sections explore the global behavior within the Earth-Moon L_2 halo family, pinpointing the challenging transition region through the utilization of the fold bifurcation. Lastly, other CR3BP models are explored with varying mass parameters, illustrating that the transition-challenging region is common feature for L_2 halo orbits within different mass ratio CR3BPs, where the fold bifurcation serves as a efficient metric to characterize the transition challenges.

II. Frame and Dynamical Models

Two dynamical models are employed in the current work. The CR3BP functions as a lower-fidelity model, while the ER3BP serves as an intermediate model to approximate the time-dependent perturbations present in the HFEM. Consistently applied in both models are point-mass representations for the celestial bodies. The dimensional gravitational parameters for these celestial bodies are denoted as $\tilde{\mu}$, where $\tilde{\mu}_E$ and $\tilde{\mu}_M$ represent values for the Earth and the Moon, respectively. These values are consistent with the JPL ephemerides, DE440.bsp [17]. A common reference frame is introduced, followed by the definition of the two dynamical models.

A. Pulsating-Rotating Frame

The pulsating-rotating frame, or the rotating frame, is employed for both model formulation and trajectory visualization throughout the current work. This frame is defined by three unit vectors: (1) $\hat{x}$ directs from the Earth to the Moon, (2) $\hat{z}$ coincides with the angular momentum vector of the celestial bodies, and (3) $\hat{y}$ completes the dextral triad. The origin of the frame is the barycenter of the Earth and Moon. Regardless of the instantaneous dimensional Earth-Moon distance (characteristic length), the frame adopts a consistent nondimensional unit, where the nondimensional Earth-Moon distance is always unity. Within the frame, the Earth, Moon, and spacecraft are associated with following position vectors,

$$\vec{r}_E = -\mu\hat{x} \tag{1}$$

$$\vec{r}_M = (1-\mu)\hat{x} \tag{2}$$

$$\vec{r}_s = x\hat{x} + y\hat{y} + z\hat{z}, \tag{3}$$

where μ denotes the mass ratio of the Earth and Moon defined as $\mu = \tilde{\mu}_M/(\tilde{\mu}_E + \tilde{\mu}_M)$. The subscripts E, M, and s denote the Earth, Moon, and spacecraft, respectively. Note that the Earth and Moon position vectors are fixed within the rotating frame on the $\hat{x}$ axis, separated by a unit nondimensional distance.

B. Circular Restricted Three-Body Problem (CR3BP)

Within the Earth-Moon CR3BP, the Earth and Moon orbit in mutual circular orbits. The third body, the spacecraft, does not influence the motion of the primaries, known as the restricted mass assumption. The spacecraft motion follows the equations of motion within the rotating frame as,

$$\ddot{\vec{r}} = -2\hat{z} \times \dot{\vec{r}} + \nabla\Omega_C \tag{4}$$

where $\times$ denotes a cross product, and Ω_C denotes the pseudo-potential function defined by $\Omega_C = (x^2+y^2)/2 + \Omega$, where $\Omega = (1-\mu)/r_{Es} + \mu/r_{Ms}$, and r_{Es} and r_{Ms} represents the non-dimensional distance between the Earth and spacecraft and between the Moon and spacecraft, respectively. The independent variable for Eq. (4) is the non-dimensional time variable t, where the dot corresponds to the differentiation with respect to t, e.g., $\dot{\vec{r}} = d\vec{r}/dt$.

C. Elliptic Restricted Three-Body Problem (ER3BP)

The ER3BP incorporates a conic motion for the Earth and Moon. The independent variable for the model is commonly adopted as the true anomaly of the Earth-Moon motion, denoted as f in the current investigation. The eccentricity of the conic is represented by e, where values between $0 \leq e < 1$ are feasible. For the Earth-Moon system, 0.055 represents a sample realistic value [10]. The spacecraft motion within the ER3BP evolves with the equations of motion within the rotating frame as,

$$\frac{d^2\vec{r}}{df^2} = -2\hat{z} \times \frac{d\vec{r}}{df} + \nabla\Omega_E, \tag{5}$$

where the pseudo-potential function for the ER3BP, Ω_E, is $\Omega_E = \Omega_C/(1+e\cos f) - (e\cos f)z^2/(2+2e\cos f)$. Note that the ER3BP reduces to the CR3BP and f also reduces to t for $e = 0$, thus, a smooth continuation is possible between the two models. Note that different formulations for the ER3BP are available in Hiday and Howell [18], cast in a non-dimensional rotating frame where the Earth and Moon are not fixed.

III. Earth-Moon L_2 Halo Orbits and Related Structures

A. CR3BP L_2 Halo Periodic Orbits (POs)

The L_2 halo family emanates from the planar L_2 Lyapunov orbit family through a pitchfork bifurcation, where the southern and northern halo families exist as a mirror configuration across the $\hat{x} - \hat{y}$ plane within the rotating frame. The current investigation focuses on the southern family for its relevance in the near future cislunar space exploration, e.g., the 9:2 NRHO. The Earth-Moon L_2 southern halo family is illustrated in the rotating frame in Fig. 2(a). The CR3BP POs are diffeomorphic to topological circles. Thus, any state on a PO is parameterized by a single angle, also denoted as the longitudinal angle, θ. The subscript 0 denotes the zero longitudinal angle, $\theta = 0°$, referenced at the apolune of each orbit. The plotted orbits in Fig. 2(a) are a subset of the family that remain above the lunar radius. Figure 2(b) illustrates the hodograph for the x position at the apolune, i.e., x_0, versus the period of the orbit in days. For dimensionalization of time, $t^* \approx 375699$ seconds is multiplied with the non-dimensional period. Note the Earth-Moon L_2 halo family admits a monotonic evolution of the period. Thus, in the current investigation, the period of the orbit is adopted as the parameter to specify each member along the family, typically visualized on the horizontal axis as displayed in Fig. 2(b).

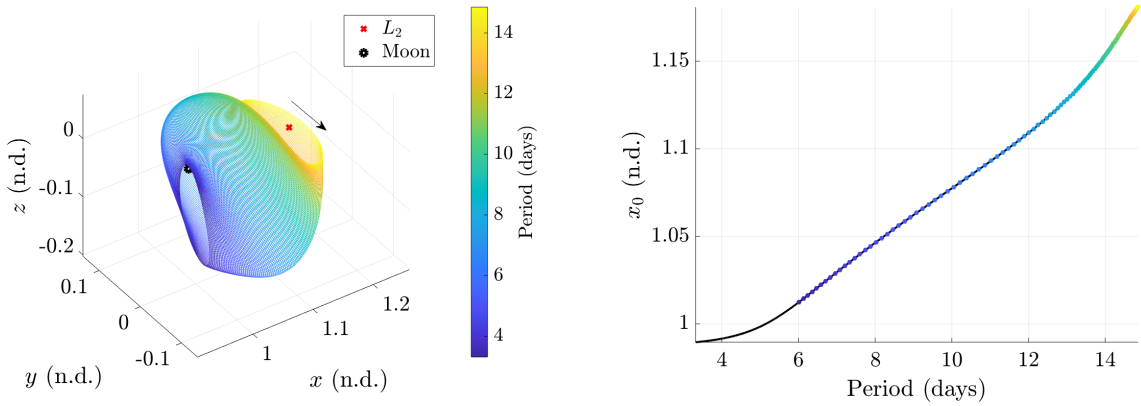

(a) Geometries within the rotating frame **(b) Family hodograph: x_0 vs. period**

Fig. 2 Earth-Moon L_2 southern halo family, recreated from Park and Howell, Figure 1. [11]

B. Nearby CR3BP L_2 Higher-Period POs and Quasi-Periodic Orbits (QPOs)

Stability information for the CR3BP PO is reviewed. The PO within the CR3BP is also represented by a constant-time mapping function, $\vec{\psi} : \mathbb{R}^6 \rightarrow \mathbb{R}^6$, that maps a fixed point to itself after one period, T. Representing the fixed point as $\vec{s} \in \mathbb{R}^6$, consisting of the position and velocity of the spacecraft as evaluated within the rotating frame, i.e., $\vec{r}$ and $\dot{\vec{r}}$, respectively, $\vec{\psi}(\vec{s}) = \vec{s}$. The monodromy matrix of is accordingly defined as $M := \frac{\partial \vec{\psi}}{\partial \vec{s}}$. The monodromy matrix contains the linear stability information for the PO and provides the information for nearby structures. As the CR3BP is a Hamiltonian system, the six eigenvalues for M occur in three reciprocal pairs. Additionally, since CR3BP is an autonomous system and the CR3BP POs exist in families with varying periods, M produces a trivial eigenvalue pair, $\lambda_{1,2} = 1$. The geometric multiplicity for this eigenvalue is 1, thus, M for CR3BP POs is always defective. The normal eigenvector for the trivial pair corresponds to the along-orbit direction, and the generalized eigenvector is associated with the family tangent direction [19, 20]. Two other reciprocal pairs are denoted as $\lambda_{3,4}$ and $\lambda_{5,6}$.

When M admits a linear center subspace, $\lambda_{3,4}$ or $\lambda_{5,6}$ reside on the unit circle within the complex plane. These center eigenvalues for POs along the L_2 halo family that remain above the lunar radius are illustrated in Fig. 3, where the vertical axis visualizes the rotation number computed as,

$$\rho = \arccos(Re(\lambda)), \tag{6}$$

with $\rho \in [0, \pi]$. Note that a slightly different definition is provided in Lujan and Scheeres [21] where ρ is defined between 0 and 2π. As the eigenvalues occur as conjugate pairs, the definition within the range of $\rho \in [0, \pi]$ also covers all possibilities. In a linear sense, ρ signifies the rotated angle within the linear center subspace for a given perturbation

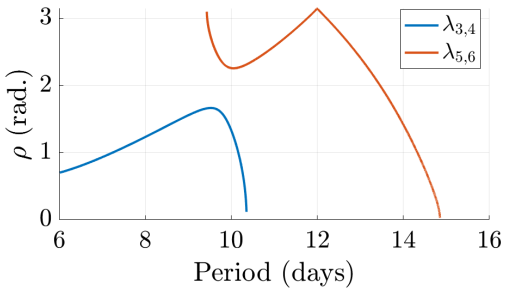

Fig. 3 The rotation number (ρ) along the family

within the subspace after one period, T. The linear center subspace is tangent to the nonlinear center manifolds that lead to bifurcations into nearby CR3BP higher-period POs or the QPOs.

When ρ is in *resonance* with 2π, or, a rational multiple of 2π, the CR3BP PO undergoes a bifurcation leading to the formation of a higher-period PO family, also known as period-multiplying bifurcations. In such instances, there exist positive coprime integers p and q satisfying $p : q = 2\pi : \rho$. An illustrative example appears in Fig. 4, depicting the period-tripling bifurcation from a location where $\rho = 2\pi/3$. In Fig. 4(a), the L_2 halo family is represented in black, with the horizontal axis corresponding to the periods of the orbits in days. To depict the intersection with the period-tripling family, the periods of the halo orbits are multiplied by three. Through the period-tripling bifurcation, a new family emerges from the original orbit where $\rho = 2\pi/3$, portrayed in red. Figs. 4(b) and 4(c) showcase two sample orbits constructed at either end of the red hodograph from Fig. 4(a). It is essential to note that, although the new family evolves with different values of period, it maintains the original rotation number, i.e., $\rho = 2\pi/3$. This behavior is evident from the fact that the orbit geometries both involve three distinct lobes. Therefore, higher-period orbit families are regarded as constant ρ branches within the CR3BP in the present investigation.

When ρ is not in resonance with 2π, or when $2\pi/\rho$ is an irrational number, the CR3BP POs undergo bifurcations leading to the formation of QPOs. Each center mode depicted in Fig. 3 yields a two-parameter QPO family, where T represents the period of the underlying halo orbit, and ρ governs the rotation number per stroboscopic mapping time, denoted as T. It is noteworthy that the family is Cantor; specifically, when ρ is in resonance with 2π, the QPOs collapse to higher-period periodic orbits. While various methods exist to define a one-parameter family or branch for QPOs [22], a constant ρ QPO branch is analogous to a higher-period PO branch. The QPOs are diffeomorphic to topological tori and involve two angular variables for parameterization. The rotation number ρ signifies the change in the latitudinal angle per stroboscopic time T, i.e., one cycle of the longitudinal angle. Notably, the longitudinal angle is associated with the underlying CR3BP PO, while the latitudinal angle originates from the center mode of the periodic orbit within the CR3BP. The significance of these nearby CR3BP structures is demonstrated in Section IV, where the continuation process within the ER3BP often connects with them.

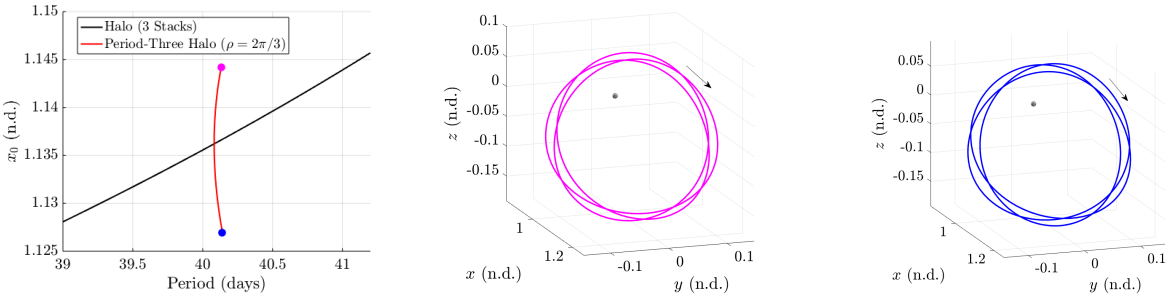

(a) Hodographs **(b) Example orbit 1** **(c) Example orbit 2**

Fig. 4 Period-tripling bifurcation example

C. ER3BP L_2 Halo Counterparts: POs and QPOs

Given that the ER3BP is a time-dependent system, the CR3BP periodic orbits (POs) typically transform into ER3BP POs and Quasi-Periodic Orbits (QPOs) with a non-zero eccentricity. Another rotation angle is introduced as,

$$\rho_E = T, \tag{7}$$

that quantifies the change in phase (representing the latitudinal angle within the ER3BP structures) per stroboscopic mapping time, T. Note that this angle is distinct from ρ as defined in the center subspace of the CR3BP PO. However, there is a possibility that the two are offset by $2k\pi$ for an integer k, a property discussed further in Section IV.B.2. Similar to the evolution of CR3BP higher-period POs and QPOs, transformation into ER3BP POs and QPOs is influenced by the resonance of ρ_E with respect to 2π.

1. ER3BP POs

In instances where ρ_E is in resonance with 2π, the CR3BP POs evolve into the ER3BP POs. As the ER3BP is a periodically perturbed system with a period of 2π with respect to the true anomaly, f, the period of the orbit needs to be commensurate with the period of the dynamics. The ER3BP POs considered in this study are characterized by the rational ratio $p:q$, where $p:q = 2\pi:T$, with p and q being positive coprime integers. For every $p:q$ ratio, Ferrari and Lavagna [23] observe that two counterparts that satisfy the mirror configuration exist in general. The trivial eigenvalue pair from the CR3BP PO, i.e., $\lambda_{1,2} = 1$, distinctively bifurcates into saddle and center pairs for each counterpart as observed by Campagnola et al. [24]. The loss of the trivial pair at $e = 0$ is intricately tied to the time-dependent nature of the dynamics. Consequently, the ER3BP POs exist as island solutions at a fixed eccentricity value. This property draws a contrast with the CR3BP POs that exist in families with varying periods. Rather, the ER3BP POs exist as "families" with varying eccentricity levels, i.e., the model itself is required to change to admit a nearby PO.

Two ER3BP PO counterparts are associated with different phasing information, f_0, or, the reference true anomaly. Recall that the subscript 0 refers to the zero longitudinal angle, $\theta = 0^\circ$, referenced at the apolune of the original CR3BP PO. For p that is odd, e.g., 3, two counterparts exist for $f_0 = 0^\circ$ and $f_0 = 180^\circ$, denoted as counterpart 'A' and 'B', respectively. An example is provided in Fig. 5 for $p:q = 3:1$, where $\rho_E = 2\pi/3$ rad. for $T = 2\pi/3$ n.d., or, approximately 9.1 days. The hodographs for two counterparts are plotted in Fig. 5(a) with the eccentricity as a function of x_0 location of the orbit. Two counterparts at $e = 0.055$ are visualized within the rotating frame in Fig. 5(b). The crossings from the two counterparts at the stroboscopic map are plotted in Fig. 5(c). The counterpart 'A' admits a perpendicular crossing at $f_0 = 0^\circ$, i.e., $y = dx/df = dz/df = 0$. Then, the subsequent crossings after T and $2T$ are marked with red circles. Similarly, the counterpart 'B' initiates from another perpendicular crossing at $f_0 = 180^\circ$ and then marks distinct crossings after each return. Note that $f_{0,A} + k \cdot T$ with an integer k, $0 \leq k \leq p-1$, corresponds to the latitudinal angle for the ER3BP POs. Crossings from two counterparts more densely fill $[0, 2\pi)$ for larger p values. For an even number p, counterpart 'A' is associated with $f_0 = 0^\circ$, but counterpart 'B' is associated with $f_0 = 90^\circ$. An example is included for $p:q = 2:1$ in Fig. 6. Note that at the stroboscopic map at $\theta = 0^\circ$, the two perpendicular crossings originate solely from the counterpart 'A'. Also, $f_0 = 180^\circ$ connects back to the counterpart 'A' and does not supply additional counterpart. Rather, counterpart 'B' is offset by 90° in f_0 at the stroboscopic map; this counterpart results in two perpendicular crossings near perilune. Thus, while general characteristics for the two counterparts remain the same, i.e., both counterparts gradually fill the latitudinal angle curve with an offseted initial f_0 value, the computational process slightly differs for an odd or even p. The computational scheme in the current work leverages a perpendicular crossing at the rotating frame $\hat{x} - \hat{z}$ plane. When p is odd, the apolune state ($\theta = 0^\circ$) along the CR3BP PO is leveraged to produce both counterparts by assigning different f_0 values. For an even number p, to utilize the perpendicular crossing scheme, perilune state ($\theta = 180^\circ$) is leveraged, intialized with zero true anomaly, to yield counterpart 'B'. From Eq. (5), note that negative eccentricity in the ER3BP dynamics result in a phase shift in by $\Delta f = 180^\circ$. Thus, two counterparts for an odd number p are connected via continuation in positive and negative eccentricity directions, but they are not connected for an even number p. In the current work, for a consistent representation, only a positive range of e is utilized, and states at $\theta = 0^\circ$ are utilized to plot hodographs. Refer to Peng and Xu [25] for more information on the computation of two ER3BP PO counterparts.

2. ER3BP Quasi-Periodic Orbits (QPOs)

When $T/2\pi$ is an irrational number, the CR3BP POs are guaranteed to evolve into the ER3BP QPOs for a sufficiently small eccentricity value [26]. While analytical boundaries for the existence of QPOs remain an unresolved issue, numerical algorithms are leveraged to approximate them. In the current work, an algorithm developed by Gómez

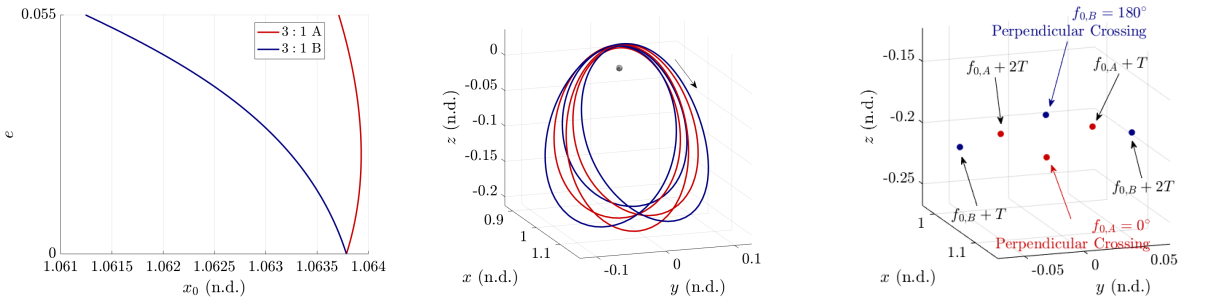

(a) Hodographs **(b) ER3BP POs at $e = 0.055$** **(c) Stroboscopic map at $\theta = 0°$**

Fig. 5 ER3BP PO example with an odd number p ($p : q = 3 : 1$)

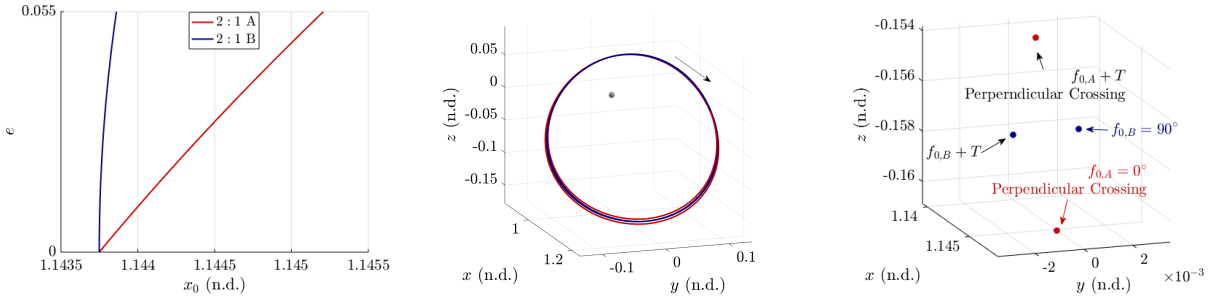

(a) Hodographs **(b) ER3BP POs at $e = 0.055$** **(c) Stroboscopic map at $\theta = 0°$**

Fig. 6 ER3BP PO example with an even number p ($p : q = 2 : 1$)

and Mondelo [27] as well as Olikara and Scheeres [28] (GMOS) is employed. This algorithm formulates a two-point boundary problem that numerically targets the *invariance condition*. For a fixed longitudinal angle at $\theta = 0°$, multiple initial conditions associated with different initial true anomalies are sampled; these initial conditions approximate the smooth, periodic invariant curve. Then, after one stroboscopic mapping time T, the final state of each trajectory remains on the same invariant curve but is rotated by ρ_E. For more information on the algorithm, refer to Olikara and Scheeres [28].

Similar to the CR3BP QPOs discussed in Section III.B, the ER3BP QPOs generally exist as a two-parameter family governed by the underlying period T, or equivalently ρ_E, and the eccentricity e. Two continuation strategies are typically employed to map out the members of this two-parameter family [29]. The first method involves continuing from each CR3BP PO and varying the model parameter e. An alternative continuation strategy adopts an evolution in ρ_E. While both approaches provide complementary search directions to fully map out the two-parameter family, the continuation in e is predominantly employed in the current work due to certain benefits. Firstly, for the POs, continuation in the rotation number is challenging, as each PO family within the ER3BP exists at discrete ρ_E values associated with different $p : q$ ratios. It is typical to vary the eccentricity for the POs, and comparing the boundaries formulated via the POs and QPOs, as demonstrated in Section IV.B, is desirable. Moreover, the ER3BP QPOs collapse to ER3BP POs for ρ_E values that are in resonance with 2π. A larger boundary in ρ_E exists near each resonant ratio, as noted by Olikara et al. [30], due to the center mode of one counterpart for $p : q$ POs. While it is possible to numerically detect and jump these resonance gaps [16], the continuation in eccentricity is less susceptible to this challenge and is considered advantageous. A continuation example is plotted in Fig. 7 for $T \approx 14.8$ days, corresponding to $\rho_E \approx 3.4$ radians. Note that 51 nodes are utilized in the current work to discretely approximate the invariant curve, as visualized in Fig. 7(c). Additionally, a single QPO covers the entire range of f at the stroboscopic map; thus, continuation in negative eccentricity does not generate different solutions, and $e > 0$ is leveraged, similar to the ER3BP PO computation.

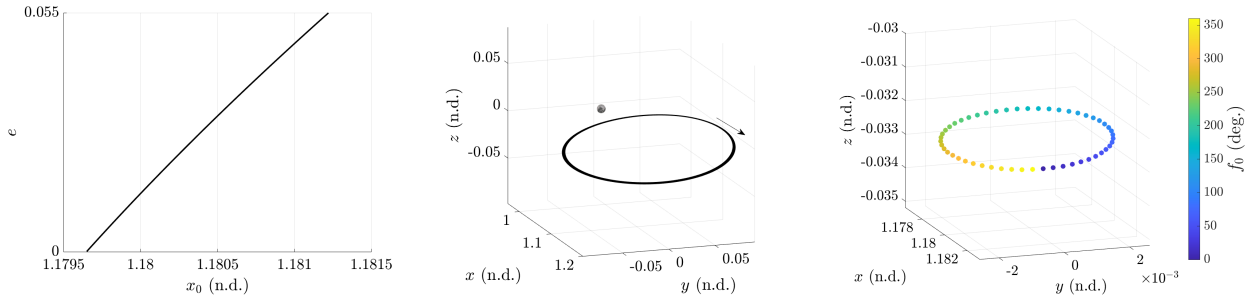

(a) Hodograph **(b) ER3BP QPO at $e = 0.055$** **(c) Stroboscopic map at $\theta = 0°$**

Fig. 7 ER3BP QPO example with $T \approx 14.8$ days

IV. Characterizing Transition-Challenging Regions with the ER3BP

Park and Howell [11] reveal that, for the Earth-Moon L_2 halo orbits, the long-term HFEM analogs emerge in the vicinity of the ER3BP QPO structures defined at a realistic Earth-Moon system eccentricity value, $e = 0.055$. Then, they demonstrate for a subset of the family corresponding to 8.6 to 11.1 days, that the ER3BP QPOs are challenging to continue to the desired eccentricity level. This region coincides with the region within the HFEM where the transition from the CR3BP is particularly challenging, associated with following two characteristics: (1) the solution geometry within the HFEM deviates significantly from the original CR3BP POs, and (2) producing long-term solutions becomes challenging.

The current work adds insight concerning the evolution of the ER3BP structures where the CR3BP to HFEM transition is particularly challenging. The focus of the investigation is the underlying dynamical factor that complicates the computation of ER3BP counterparts at the realistic eccentricity value of $e = 0.055$. This section introduces two representative bifurcation behaviors that distinguish between a nominal behavior, i.e., the CR3BP POs transition readily to the HFEM, and a challenging case. Such behaviors are validated within a global context across the Earth-Moon L_2 halo family in Section V.

Two bifurcation diagrams appear in Fig. 8, illustrating two representative behaviors reflecting the evolution of any CR3BP PO into the corresponding ER3BP structures, either the PO or QPO. Note that the three axes constitute a generic three-dimensional hodograph to depict the evolution of relevant structures. In the original L_2 halo orbit within the CR3BP ($e = 0$), the family evolves with the fixed point $\vec{s} \in \mathbb{R}^6$ and the associated period, T. For the fixed point, the reference longitudinal angle of $\theta = 0°$ is consistently utilized. The third axis in the plot corresponds to the eccentricity, e. Following the discussions from Section III.C, only $e \geq 0$ is employed to represent the evolution of structures. Note that the bifurcation diagrams are applicable to both the ER3BP POs and QPOs.

A. Nominal Case (Fig. 8(a))

For the nominal case, the ER3BP structures that emanate from the CR3BP are readily continued to the realistic eccentricity value, $e = 0.055$, without a *turn* in eccentricity (yellow in Fig. 8(a)).

1. CR3BP → ER3BP Bifurcation (★)

The dynamical evolution of the ER3BP structures for the nominal case is characterized by a single bifurcation, denoted as ★. The ER3BP branch originates from the bifurcation of the original CR3BP family at ★, initiated by the loss of the trivial eigenvalue pair, $\lambda_{1,2} = 1$. The continuation process along the yellow branch assumes a constant stroboscopic mapping time T, as illustrated by the grey surface in Fig. 8(a). The rotation number ρ_E also remains constant for this branch, governed by the ER3BP dynamics. Subsequently, the nominal case demonstrates a monotonic increase in eccentricity until the continuation process reaches $e = 0.055$..

2. Example - ER3BP 13 : 7 PO and a Nearby QPO

For illustration, consider a ER3BP PO that is associated with a resonant ratio, 13 : 7. In this case, the stroboscopic mapping time is fixed as $T = 7 \cdot 2\pi/13 \approx 3.383253$ n.d.. The three-dimensional hodograph is plotted in Fig. 9, where the x-axis of the plot corresponds to x_0 at $\theta = 0°$, and the other two axes denote T and e, respectively, consistent with

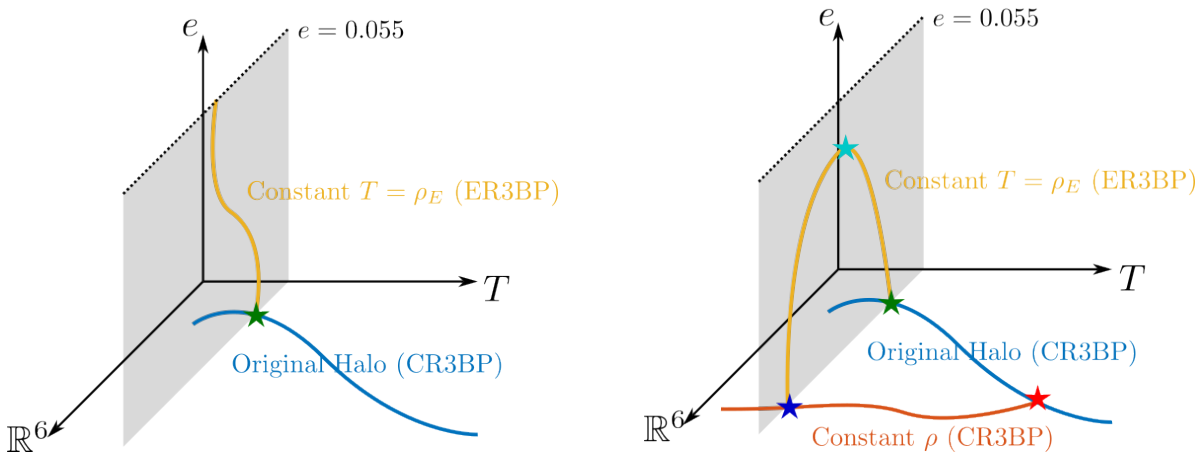

(a) Nominal case **(b) Fold bifurcation**

Fig. 8 Two representative bifurcation diagrams

the notation from Fig. 8(a). Note that two counterparts bifurcate from the same point (★) for the POs, corresponding to two separate lines as depicted in Fig. 9. As p is an odd number, $p = 13$, the second counterpart corresponds to an initial true anomaly of $f_0 = 180°$. Subsequently, a nearby QPO associated with a fixed $T \approx 3.383250$ n.d. is also continued. Since the invariant curve for the QPO spans all f_0 angles between 0° and 360°, $f_0 = 0°$ and $f_0 = 180°$ are selected for comparison with the two counterparts for the 13 : 7 POs. Visually, it is evident that the nearby QPO closely approximates the hodographs traced by the two counterparts for the POs. This particular resonance ratio corresponds to approximately 14.7 days and is far from the predescribed transition-challenging region. Thus, the nominal behavior manifests, wherein both the PO and QPO hodographs continue to $e = 0.055$ without a turn in eccentricity.

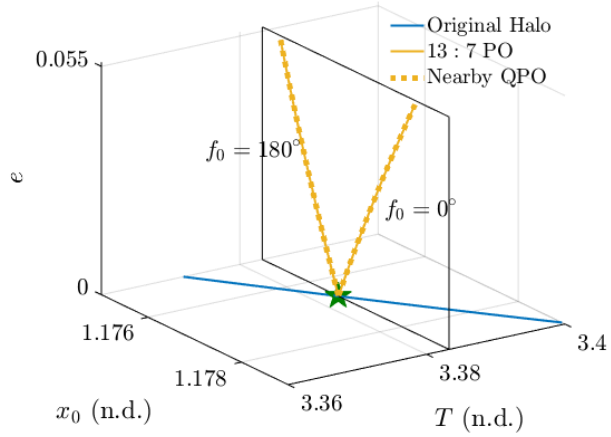

Fig. 9 Nominal case: 13 : 7 PO and a nearby QPO bifurcation diagrams

B. Fold Bifurcation (Fig. 8(b))

A more complex scenario commonly occurs in the region where the CR3BP to HFEM transition is particularly challenging, involving the fold bifurcation. An illustrative case is presented in Fig. 8(b), showcasing four distinct types of bifurcations visualized with different colors (★, ★, ★, ★). As the first type of bifurcation (★) is common in both cases depicted in Figs. 8(a) and 8(b), explanations are provided for the other three bifurcations.

1. Fold Bifurcation (★)

In a more general sense, a fold bifurcation is a type of tangent bifurcation where a stability change occurs as an eigenvalue pair for the monodromy matrix M passes through +1 within the complex plane. However, located at an extremum, it does not result in the generation of a new family of solutions. When a new family is generated, transcritical or pitchfork bifurcations occur, facilitating an intersection between the old and the new families. In the current work, a fold bifurcation refers to a *turn* in the eccentricity, or, as demonstrated in Fig. 8(b), a local extremum in eccentricity along the hodograph. As discussed in Appendix VIII.A, whenever this local extremum behavior is observed, the eigenvalue for the monodromy matrix admits a unity pair, with the eigenvector coinciding with the local family tangent direction as depicted in the hodograph.

2. Resonance Bifurcation (★)

After a turning point (★), it is possible for the ER3BP family to evolve back to zero eccentricity, connecting to a distinct CR3BP solution that differs from the original bifurcating point, i.e., ★≠★. This bifurcation is labeled as a "resonance bifurcation" because the rotation numbers provided by the ER3BP and CR3BP dynamics are in resonance at this bifurcation point, i.e., $\rho = \rho_E + 2k\pi$ for an integer k. Through this process, a new family within the CR3BP is exposed, highlighted in red in Fig. 8(b). It is possible to continue this family within the $e = 0$ plane, now allowing T to change, corresponding to the CR3BP PO or QPO branch with a fixed rotation number, ρ.

3. Period-Multiplying (PO) / Hopf (QPO) Bifurcation (★)

It is possible that the constant ρ branch within the CR3BP continues back to the original halo orbit family, connected via a bifurcation at ★. For the periodic orbits, this bifurcation corresponds to a period-multiplying bifurcation where ρ is in resonance with 2π. In constrast, when ρ is not in resonance with 2π, the bifurcation is denoted as Hopf, secondary Hopf, or Naimark-Sacker bifurcations [31].

4. Significance within the Context of HFEM Transition

Recall that the HFEM analogs for the Earth-Moon L_2 halos evolve in the vicinity of the ER3BP structures at a realistic eccentricity level, e.g., $e = 0.055$. The fold bifurcation, as depicted in Fig. 8(b), illustrates one possible dynamical behavior that impedes the computation of the ER3BP structures at the desired eccentricity value at $e = 0.055$ and, hence, the characterization of the HFEM analogs. In the representative bifurcation behavior in Fig. 8(b), the continuous family within the ER3BP in yellow does not reach $e = 0.055$ without connecting back to $e = 0$. This trait implies that a successful smooth transition process may be required to leverage a nearby period-multiplied PO or a QPO associated with the center mode of the original CR3BP halo orbit, indicating that the CR3BP PO itself potentially does not serve as a suitable initial guess for the transition process.

5. Relationship to Broken Bifurcations

Perfect transcritical or pitchfork bifurcations allow an intersection of two continuous families that share a common member at the intersection point. The term broken bifurcations denotes cases where these perfect intersections, typically under a perturbation parameter [31], are destroyed, resulting in two continuous branches that are disconnected. This behavior is commonly reported in various four-body restricted body problems in multiple investigations [14, 16, 30, 32, 33]. In the current work, such behavior is also confirmed within the ER3BP, and its relationship to the fold bifurcation is illustrated.

Periodically perturbed systems, including the ER3BP, are generally cast as one-parameter dynamical models. For the ER3BP, with a fixed μ value, the dynamics are governed by a single parameter, e. Seydel [31] notes that while fold bifurcations are "generic" (most typical) for one-parameter models, perfect family intersections from perfect transcritical or pitchfork bifurcations may only exist when some peculiar symmetry is satisfied. Within the CR3BP at a fixed μ value, considered a zero-parameter model, these perfect bifurcations are more commonly observed (e.g., pitchfork bifurcation from planar Lyapunov orbits to southern and northern halo orbits). On the contrary, these family intersections are expected to exist more sparsely within the ER3BP, only when some symmetry properties are provided. In a similar context, Jorba et al. [33] also point out that the lack of symmetry within four-body models may destroy the intersection, resulting in broken bifurcations. More insights are provided in the Appendix (VIII.B) on the evolutions of the smooth families within a periodically perturbed Hamiltonian system that likely result in broken bifurcations rather than perfect family intersections.

Broken bifurcations are critical in understanding the challenges of transitioning from the CR3BP to HFEM. A smooth continuation process may actually lead to a fundamental change in behavior, deviating from the desired solution geometry of the original CR3BP structure. Detecting broken bifurcations, however, is a non-trivial task. Since broken bifurcations involve a smooth family evolution by definition, additional information is necessary to confirm their existence. Potential strategies include exploring different continuation directions [15], introducing additional perturbation parameters [15], and measuring the curvature of the hodograph [16]. Seydel [31] acknowledges the general challenges associated with such processes. In the current work, the fold bifurcation is employed as a practical metric to identify potential transition challenges from the CR3BP to the HFEM. Note that the fold bifurcation is not equivalent to broken bifurcations. Broken bifurcations do not necessarily involve a fold in eccentricity, and the presence of a fold bifurcation alone does not confirm a broken branch. However, in cases where the fold bifurcation eventually reaches back to zero ($e = 0$), as commonly observed in the Earth-Moon L_2 halo family, the hodograph exhibits at least one broken bifurcation. This broken bifurcation links the original CR3BP halo family to a distinct CR3BP structure associated with the constant ρ branch.

6. Example - ER3BP 53 : 21 PO and a Nearby QPO

llustrative bifurcation diagrams are presented in Fig. 10. The solid yellow line in the plot represents a resonant ratio PO with $p : q = 53 : 21$ associated with $T \approx 2.48956$ n.d., and the dotted markers indicate a nearby QPO associated with $T \approx 2.48963$ n.d.. Both counterparts for $f_0 = 0°$ and $f_0 = 180°$ exhibit a folding bifurcation, ★. It is noted that the local extrema eccentricity values for the two counterparts differ slightly in general. Following the folding bifurcations, the ER3BP structures return to the CR3BP plane, i.e., $e = 0$, bifurcating to the CR3BP branch (★) through the resonance bifurcation. Tracking this CR3BP branch in red within Figure 8(b), the structure reconnects with the original CR3BP L_2 halo family through either a period-multiplying or the Hopf bifurcation (★). Similar to the nominal case depicted in Figure 8(a), the resonant ratio PO and a nearby QPO exhibit similar behavior in terms of hodographs.

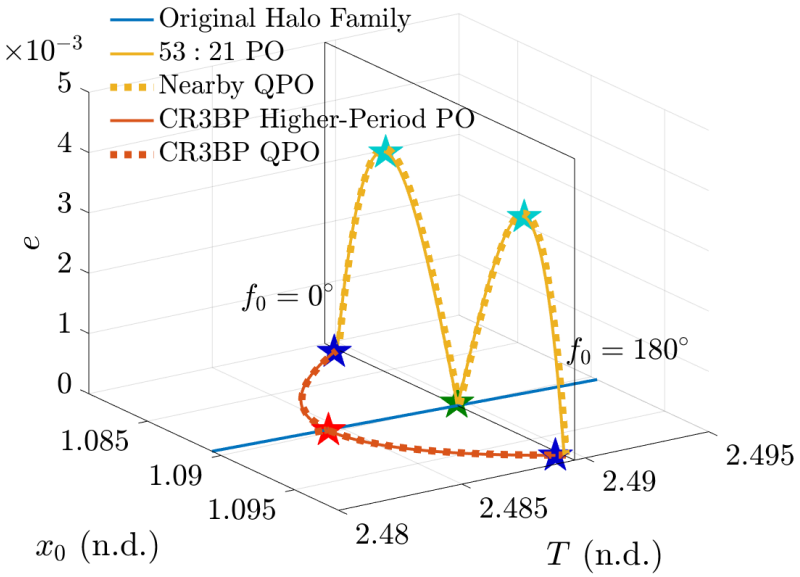

Fig. 10 Fold bifurcation: 53 : 21 PO and a nearby QPO bifurcation diagrams

C. Additional Scenarios

While two illustrative cases are discussed, it is important to note that other cases do exist that exhibit more complex bifurcation behavior and do not precisely adhere to the two patterns visualized in Fig. 8. Some of these additional cases and their implications for the HFEM transition process are examined.

Firstly, the continuation process occasionally reaches $e = 0.055$ but with a non-zero, even number of fold bifurcations. An example is illustrated in Fig. 11, corresponding to the 14 : 5 ratio PO, counterpart 'A'. It is observed that two fold

bifurcations appear along the continuation process, marked with ★; however, the evolution is continuous and reaches the desired $e = 0.055$ at the end. Consequently, this case does not align with either of the scenarios described in Fig. 8. For this specific case, it is not immediately clear whether a broken bifurcation occurs leading to a nearby CR3BP structure. It is worth noting that this case is rarely found within the Earth-Moon L_2 halo family.

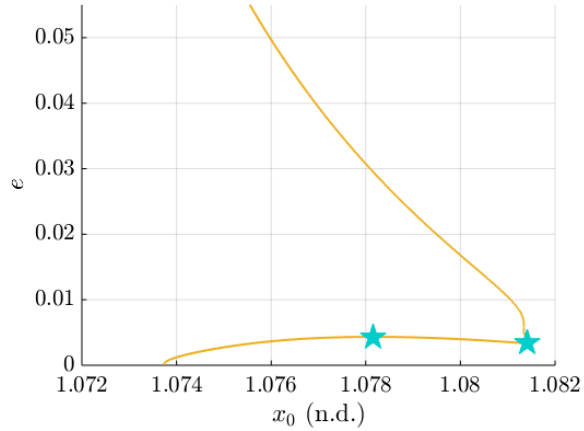

Fig. 11 14 : 5 **PO counterpart 'A', even number of fold bifurcations**

The two PO counterparts typically exhibit similar behavior in terms of two representative bifurcation patterns, where the shapes of the hodographs are generally similar and typically involve fold bifurcations at approximately equivalent eccentricity values. However, this similarity is not guaranteed. An example illustrating this variation is provided in Fig. 12 that showcases two counterparts for the 29 : 10 PO. Notably, the two counterparts exhibit very distinct behavior within the hodograph, with differences in the first fold bifurcation eccentricity value and the total number of fold bifurcations. Moreover, the second counterpart displays much more complex bifurcation behavior. While the diagrams in Fig. 8 illustrate *representative* cases, more complex behaviors occasionally exist. Similar intricate behavior is expected for the CR3BP constant ρ branch, corresponding to the red curve within Fig. 8(b). This branch may also undergo multiple bifurcations before ultimately reaching the original CR3BP halo family within the hodograph. The potential complexity of bifurcation behavior underscores the necessity for a simple metric, with the fold bifurcation emerging as a practical tool.

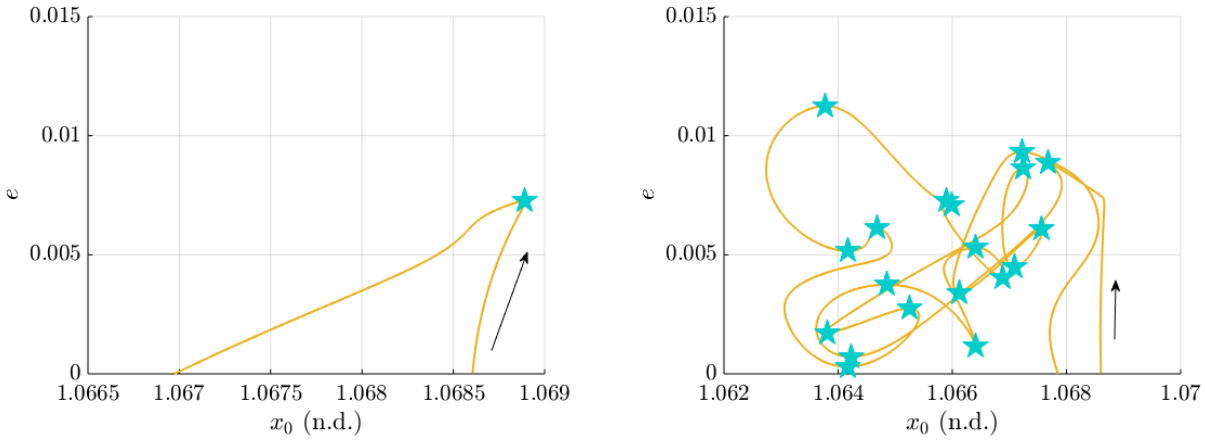

(a) Counterpart 'A' **(b) Counterpart 'B'**

Fig. 12 29 : 10 **PO, two counterparts with distinct hodographs**

D. Numerical Challenges

The detection of the fold bifurcation is contingent on the specific numerical continuation formulations. The present work utilizes a perpendicular crossing for the continuation process in the evolution of ER3BP POs, assuming that the family members evolve while reflecting a mirror configuration across the $\hat{x} - \hat{z}$ plane. Eliminating this assumption potentially reveals more fold bifurcations that connect to non-symmetric structures. Additionally, a denser step size in the continuation process potentially exposes more broken bifurcations. An example is illustrated for the 73 : 24 ratio ER3BP PO in Fig. 13, where three different branches are located with three different step sizes. Leveraging larger step sizes often "jumps" between the broken branches and does not detect them, as demonstrated by Branch 3. On a similar note, natural parameter continuation procedure, as opposed to pseudo-arclength continuation, is more capable of jumping between disconnected branches in general. Thus, defining "true" bifurcation diagrams is challenging due to the multiple factors in the numerical procedure. However, qualitative analysis on the proliferation of broken bifurcations, or alternatively, fold bifurcations, remains possible.

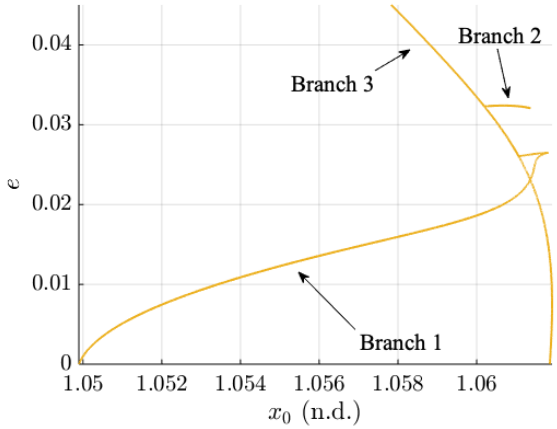

Fig. 13 73 : 24 **PO counterpart 'A', different branches located via different step sizes**

While the ER3BP QPOs exhibit similar behavior to the nearby ER3BP POs, as demonstrated via a sample ratio as illustrated in Fig. 10, QPO computation often encounters challenges prior to reaching the exact fold bifurcation. A numerical limit for QPO computation generally arises when invariant curves become too complex [11] to be accurately represented by a finite number of discretized points. An example is illustrated for $p : q = 59 : 21$ and a nearby QPO in Fig. 14. While both hodographs display similar behavior, the QPO computational limit is reached before the PO fold bifurcation (★). Although using different numbers for invariant curve discretization locally alleviates the problem, QPO continuation typically fails eventually, as approaching the fold bifurcation typically involves a qualitative behavioral change in the structures where the invariant curves become complex for the employed GMOS QPO computation algorithm. Thus, while both POs and QPOs are leveraged in the current work to provide a more holistic investigation, POs generally offer more accurate bifurcation information, and QPOs complement the information from the PO analysis.

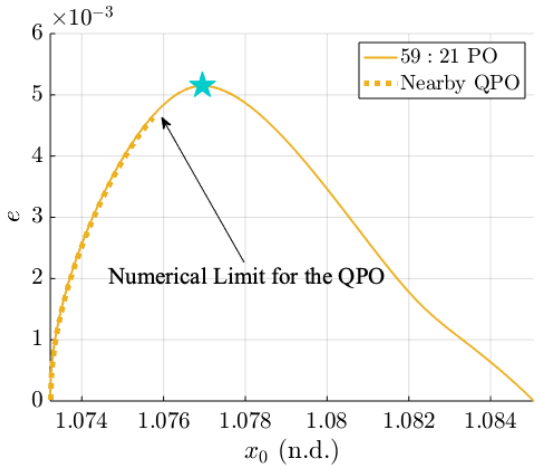

Fig. 14 59 : 21 **PO counterpart 'A' and a nearby QPO**

V. Transition-Challenging Regions within the Earth-Moon L_2 Halo Family

A. Global Trend for Fold Bifurcations across the Family

The bifurcation behavior for the Earth-Moon L_2 halo family is globally examined, focusing on the existence of fold bifurcations. The global trend across the family is depicted in Fig. 15, with the corresponding $p:q$ values within the ranges identified in Table 1. Different combinations of $p:q$ that result in coprime numbers are selected. The CR3BP halo orbits corresponding to these resonant ratios are continued with the numerical scheme outlined in Appendix (VIII.C). The vertical axis of the plot corresponds to the range of e values under consideration, with the maximum value set at $e = 0.055$. Note that each PO ratio has two counterparts, and these counterparts may exhibit unique bifurcation behavior, as noted in Fig. 12. Cyan markers (★) denote the minimum first fold bifurcation eccentricity for both counterparts. In cases where only one of the counterparts exhibits a turn in eccentricity, that specific eccentricity is marked. If both counterparts undergo fold bifurcations, the smaller eccentricity value from the two turning eccentricity values is marked. Two yellow markers indicate $p:q$ ratios where both counterparts reach $e = 0.055$ at the end of the coninuation process. The first type (●) achieves $e = 0.055$ without any fold bifurcation as illustrated in Fig. 9. The second type (★) involves an even number of fold bifurcations until the continuation process reaches $e = 0.055$ as depicted in example in Fig. 11. For some higher numbers of p, the continuation procedure occasionally diverges due to numerical sensitivities. Such cases are not plotted in Fig. 15.

The intermediate region from $T = 8.6$ to 11 days are characterized by the existence of fold bifurcation (★) at $e < 0.055$ and the evolution back to zero eccentricity. Beyond this period range, the yellow markers (●) govern the behavior, i.e., this continuation scheme reaches $e = 0.055$ without any fold bifurcations. Generally, these markers for the PO continuation align well with adjacent QPO eccentricity boundaries, colored in grey. The QPO boundaries note the maximum eccentricity value before the continuation exhibits a turn in eccentricity or fails to converge due to the complex shape of the invariant curve. In Fig. 15, for the regions where QPOs successfully continue up to $e = 0.055$, the yellow markers (●) proliferate, and vice versa. Note that the vertical gaps in the QPO continuation process correspond to the resonance gaps as discussed in Park and Howell [11] as well as Olikara et al. [30]. From Fig. 1, these yellow markers (●) correspond to the regions where multi-year HFEM counterparts are readily computed with the CR3BP orbit geometry as the initial guesses. **Therefore, the proliferation of ER3BP PO fold bifurcations before reaching $e = 0.055$ successfully predicts challenges in HFEM transition.** Alternatively, similar behavior is inferred from QPO continuation boundaries. For the Earth-Moon L_2 halo family, this transition-challenging region corresponds to orbital periods between 8.6 and 11 days.

While the majority of cases adhere to the described pattern, there are exceptions that deviate. Some instances exist outside the challenging domain where fold bifurcation still occurs at $e < 0.055$. For example, the $p:q = 9:2$ displays this behavior, where one counterpart at $T \approx 6.07$ days folds at $e \approx 0.04$, despite being outside the problematic region. Upon closer examination of the transition-challenging region in Fig. 16, certain $p:q$ ratios indeed reach $e = 0.055$ without reverting to zero eccentricity. For instance, the ratio near $T \approx 9.1$ days corresponds to the 3 : 1 resonance, allowing both counterparts to reach $e = 0.055$ without encountering fold bifurcations (●). Additionally, between 9.5

and 10 days, four yellow markers (★) indicate instances where one of the counterparts reaches $e = 0.055$ with an even number of fold bifurcations. It is worth noting that the QPO boundaries exhibit slight deviations from the PO fold bifurcations, particularly for $T < 9$ days, where the QPO continuation strategy achieves higher eccentricity values as compared to the PO continuation. This discrepancy is attributed to the presence of multiple broken branches, and the effective step sizes between the PO and QPO continuation processes are marginally different. Consequently, both continuation processes may trace "continuous" branches from potentially multiple broken branches, as illustrated in Fig. 13. Despite these exceptions and numerical challenges, it remains noteworthy that the *proliferation* of fold bifurcations within the ER3BP is anticipated to signal challenges in the CR3BP to HFEM transition process.

Table 1 Range for $p : q$ values

Periods (days)	Range for p	Range for q
$T < 8.6$	$p \leq 60$	$q \leq 30$
$8.6 \leq T \leq 11$	$p \leq 100$	$q \leq 50$
$11 < T$	$p \leq 50$	$q \leq 25$

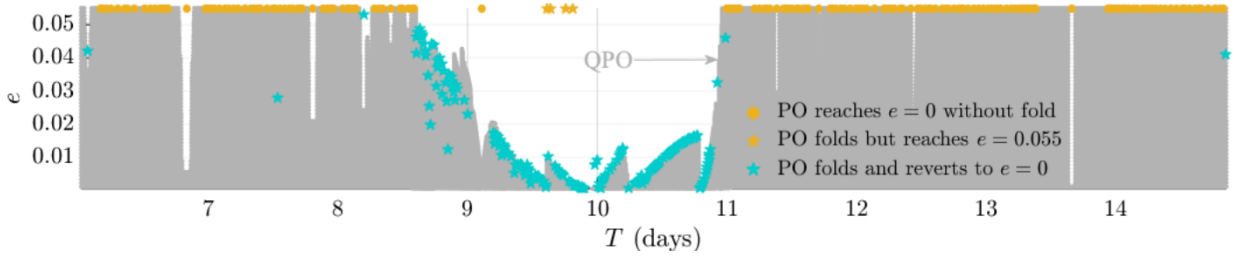

Fig. 15 Global trend across the Earth-Moon L_2 halo family

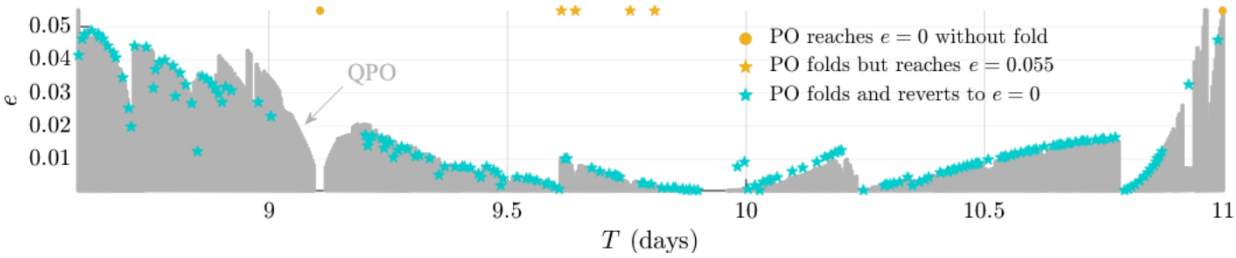

Fig. 16 Global trend across the Earth-Moon L_2 halo family: zoomed-in view

B. Fold Bifurcations at Higher Eccentricity Values

While the desired eccentricity value, $e = 0.055$, represents a realistic Earth-Moon system value, it is possible to further continue from the yellow markers (●) in Fig. 15 until the first fold bifurcation is located for each ratio. The outcomes are depicted in Fig. 17, illustrating that all ratios exhibit turns in eccentricity before $e = 0.99$, or a value near unity. It is expected that these ER3BP structures are eventually linked back to the nearby CR3BP POs as generally depicted in Fig. 8(b). The transition-challenging region in the Earth-Moon L_2 halo family, located between 8.6 and 11 days, exists as a specific area where these fold bifurcations occur *before* reaching the desired eccentricity value, $e = 0.055$, thus, resulting in some numerical transition challenges from the CR3BP to HFEM. It is also noteworthy that the NRHO region ($T < 8.6$ days) is characterized by smaller values of eccentricity at the fold bifurcations as compared to the region defined by $T > 11$.

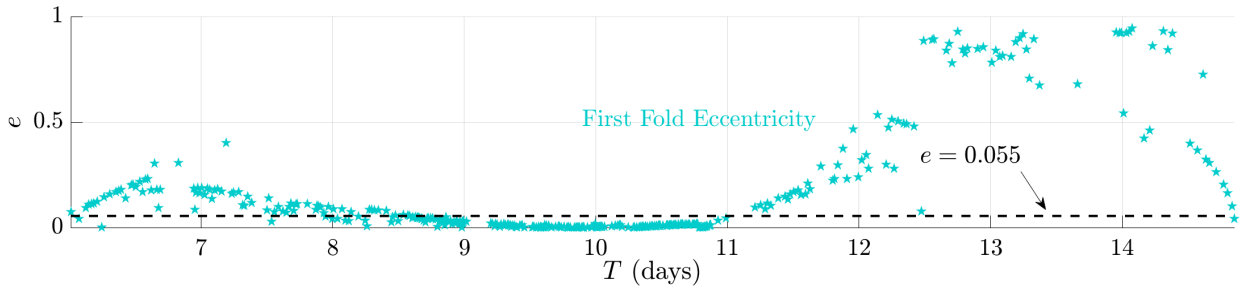

Fig. 17 First fold bifurcation eccentricity values across the family at higher eccentricity values

C. Potential Mitigation Strategies

The transition-challenging region is defined by a proliferation of fold bifurcations that impedes the computation of the ER3BP counterparts at a desired eccentricity value, i.e., $e = 0.055$. In encountering these fold bifurcations, the following strategies emerge as alternatives to produce ER3BP structures at $e = 0.055$ that potentially serve as updated initial guesses for the HFEM transition process.

1. Leveraging Nearby CR3BP Structures

After the ER3BP continuation process returns back to $e = 0$, it bicurates to a nearby CR3BP PO (★ in Fig. 8(b)). Utilizing this neighboring structure as a starting point allows for continuation in e, resulting in a hodograph as depicted in Fig. 18(a). Following the fold bifurcation (★), the continuation process returns to $e = 0$, where the bifurcation into a nearby CR3BP higher-period PO occurs (★). Another branch is then continued, eventually reaching $e = 0.055$ at ●. It is noteworthy that at ★, the initial true anomaly, f_0, is shifted from 0° to 180° to enable the computation of the new branch. The orbit geometry at the end of continuation process corresponding to $e = 0.055$ is plotted in Fig. 18(b). It is possible to employ a similar process for the turned structures that frequenctly occur in Fig. 15; obtaining nearby CR3BP POs and their corresponding counterparts within the ER3BP at $e = 0.055$ is possible and may serve as a better initial guess for HFEM analogs. However, these nearby structures are inherently associated with multiple lobes as apparent from Fig. 18(b) that typically spread in the $\hat{y}$-direction that may destroy the favorable orbit structure that the original CR3BP halo orbit offers. Refer to Peng and Hao [34] for more information regarding the Sun-Mercury system and the corresponding 5 : 2 ER3BP PO behavior.

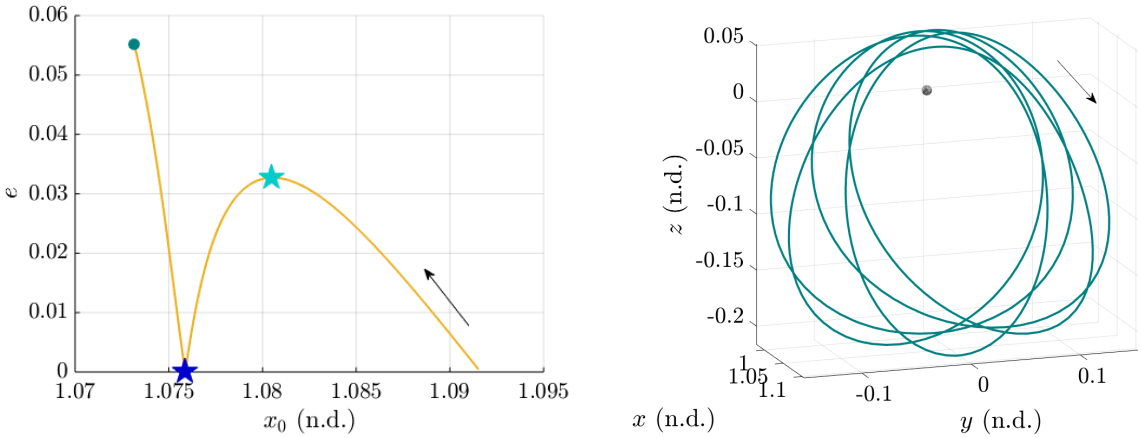

(a) 5 : 2 counterpart 'A' hodograph **(b) Orbit geometry at ● ($e = 0.055$)**

Fig. 18 5 : 2 continuation leveraging a nearby CR3BP higher-period PO

2. Jumping to the Other Broken Branch

As an alternative to the proceeding approach, it is possible to deliberately jump to the other broken branch, *potentially* existing throughout a higher range in e that continues to a value $e = 0.055$. This behavior is illustrated in Fig. 19 for the $p : q = 19 : 6$ ratio counterpart 'A'. With the original continuation scheme, only the yellow branch is located. Near the fold bifurcation (★), the sharp turn implies the presence of the other branch; a natural parameter continuation with respect to the eccentricity, instead of the pseudo-arclength continuation scheme, is leveraged to locate the other broken branch, as indicated by the arrow denoting the jumping direction. The geometry is successfully pinpointed at $e = 0.055$ with this strategies, as plotted in Fig. 19(b). Although multiple authors [15, 16] offer methods to locate the broken branches, the branch may not exist at all. Seydel [31] further emphasizes the element of chance, stating that "good luck is also needed," as the existence and location of the other branch are not known *a priori*. Thus, while the results within Fig. 19 illustrate one successful example, it may not always work for other ratios that exhibit fold bifurcations. Further backgrounds are provided in Appendix (VIII.B).

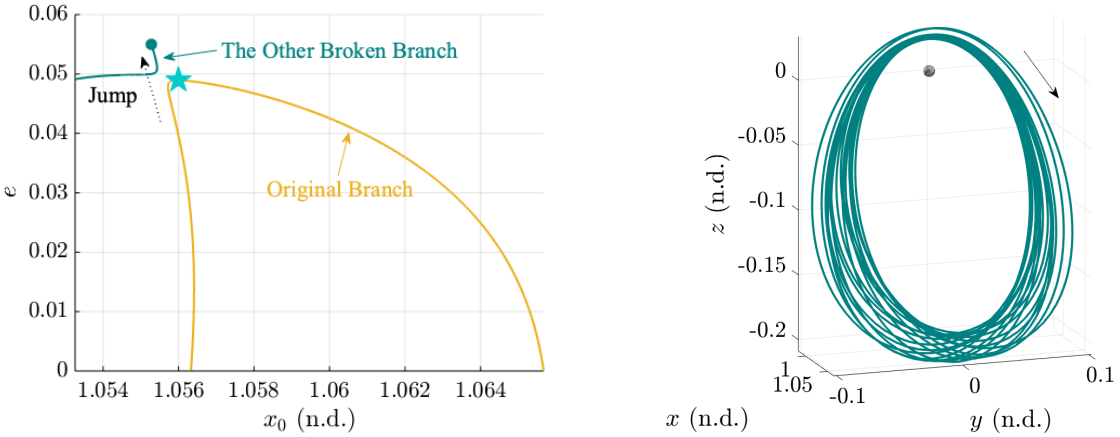

(a) 19 : 6 **counterpart 'A' hodograph** **(b) Orbit geometry at ● ($e = 0.055$)**

Fig. 19 19 : 6 **jumping to the other broken branch**

3. Continuation in μ

While the current investigation assumes that the μ parameter is fixed within the ER3BP, it also serves as an additional modeling parameter. This extra dimension introduces a distinct continuation direction, allowing different branches to connect at various μ values. Illustrated in Fig. 20 is an example where three different μ values are explored to demonstrate varying bounding eccentricity values within the transition-challenging period range, as zoomed in Fig. 16. The selected values are $\mu = 0.1$ (approximately the Pluto-Charon system), $\mu \approx 0.0125$ (the Earth-Moon system value), and $\mu = 0.001$ (approximately the Sun-Jupiter system). Although smaller μ values are more common for Sun-planet and planet-moon systems within the solar system, these three values are selected in proximity to the Earth-Moon system value. The markers in Fig. 20 depict the end of the continuation process: if a fold bifurcation is located for either counterpart before reaching $e = 0.055$, such a value is marked. If the continuation reaches $e = 0.055$, it is also marked. The plots demonstrate that the bounding eccentricity values are slightly altered for different μ values, as expected. However, the proliferation of fold bifurcations in the vicinity of the original range in period is common for these nearby μ values. The larger μ value appears to shift the fold bifurcations to higher e values, and conversely, the smaller μ value results in a shift to lower e values. While this example hints at the potential usefulness of an additional search direction in μ, further investigation is required to validate its effectiveness in providing ER3BP structures at $e = 0.055$ for the Earth-Moon system mass ratio, $\mu \approx 0.0125$.

4. Continuation in T

The fold bifurcations in Fig. 16, or the bounding eccentricities, are determined through a continuation procedure in e, where a continuation in T may assist in connecting to higher eccentricity values. Note that this strategy is potentially useful for the QPO computation, but may not be applicable for the PO computation as the POs exist at discrete $p : q$ ratios

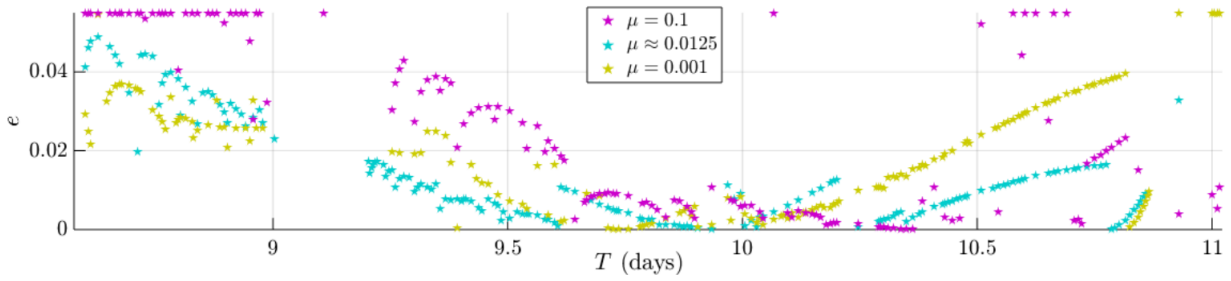

Fig. 20 Three different sample μ values for $8.6 \leq T \leq 11$ days

that do not allow continuation in T. Alternatively, other periodically perturbed models, aside from the ER3BP, facilitate continuation in T, even for the POs. For instance, the Hill Restricted Four-Body Problem [14] scales the independent variable itself as a function of the sidereal to synodic periods as the model parameter m varies; this parameter controls the pulsation of the Earth-Moon system and changes T as well [14, 15]. A continuation in T within the ER3BP may or may not be linked the continuation of the model parameter m within the HR4BP and further study is warranted.

VI. Concluding Remarks

The ER3BP's bifurcation behavior is a crucial metric for addressing the transition-challenging dynamics from the CR3BP to HFEM. In the Earth-Moon system, the proliferation of fold bifurcations before $e = 0.055$ is identified as a key behavior, illustrated within the L_2 halo family. In the period range where $8.6 \leq T \leq 11$ days, fold bifurcations frequently manifest at $e < 0.055$, creating continuous connections between ER3BP structures and nearby CR3BP structures. This region aligns with the previously identified transition-challenging area by various authors. Therefore, fold bifurcations within the ER3BP prove to be an effective metric for anticipating transition challenges within the ER3BP alone, eliminating the need for extensive numerical transition tests from the CR3BP to the HFEM.

To further validate the current findings, a number of steps are essential. Firstly, exploring the relationship with other periodically perturbed models is expected to enhance the understanding regarding the existence of broken branches and their links to CR3BP structures. Although a few sample orbits illustrate their links to CR3BP structures, further analysis is required to identify specific branches within the CR3BP. The proposed metric, the proliferation of fold bifurcations within the ER3BP, is planned for verification across various orbital families within the Earth-Moon or other systems. Additionally, in cases where a direct transition from the CR3BP to HFEM is challenging due to the abundance of fold bifurcations, the effectiveness of the proposed mitigation strategies is intended to be demonstrated in providing updated initial guesses.

VII. Acknowledgements

The first author would like to thank Kwanjeong Educational Foundation for the financial support. Valuable discussions with past and former members from Multi-Body Dynamics Research Group, including Rohith Reddy Sanaga and Dale Williams, are appreciated. Portions of this work are also supported by Purdue University and under Grant NASA JSC 80NSSC18M0122.

VIII. Appendix

A. Eigenstructure of the Monodromy Matrix at a Fold Bifurcation

When the hodographs from a family of ER3BP POs demonstrates a local extrema, the eigenstructure of the monodromy matrix, M, includes a unity eigenvalue pair at that exact location. First, an augmented fixed point for the ER3BP PO is denoted as $\vec{s}'(\gamma)$, where γ corresponds to an arbitrary monotonically evolving parameter that governs the family evolution, e.g., an arclength defined along a hodograph from the initial bifurcating point from the CR3BP PO (★ from Fig. 8). Note that the vector is seven-dimensional, i.e., $\vec{s}' \in \mathbb{R}^7$, including the state and the eccentricity associated

with each fixed point. Thus,

$$\vec{s}'(\gamma) = \begin{bmatrix} \vec{s}(\gamma) \\ e(\gamma) \end{bmatrix}, \tag{8}$$

where $\vec{s}(\gamma)$ and $e(\gamma)$ corerspond to the six-dimensional fixed point state and the eccentricity of the model, respectively. Then, assume that at $\gamma = \gamma^*$, a turn in eccentricity occurs. (The asterisk denotes the turn location.) The nearby fixed point is then represented as,

$$\vec{s}'(\gamma^* + \delta\gamma) = \vec{s}'^* + \delta\vec{s}' \approx \vec{s}'^* + \begin{bmatrix} \delta\vec{s} \\ 0 \end{bmatrix}, \tag{9}$$

where δ denotes a small increment. Then, consider an augmented periodic mapping function $\vec{\psi}'(\vec{s}') = \vec{s}'$ with a fixed period corresponding to $T = 2\pi q$ for a resonant ratio $p : q$. The seven by seven monodromy matrix M' is defined as $M' = \frac{d\vec{\psi}'}{d\vec{s}'}(\vec{s}')$. While $\vec{\psi}'$ is a time-dependent function, the initial true anomaly is fixed as f_0 and does not explicitly appear as an additional parameter. The structure of the augmented monodromy matrix M' is,

$$M' = \begin{bmatrix} M & \frac{\partial\vec{\psi}}{\partial e}(\vec{s}) \\ 0_{1\times 6} & 1 \end{bmatrix}, \tag{10}$$

where the upper left matrix is the six by six monodromy matrix and the bottom right is always unity, as the eccentricity does not depend on the state, $\vec{s}$. Then, for the nearby fixed point, the mapping function results in,

$$\vec{\psi}'(\vec{s}'^* + \delta\vec{s}') = \vec{s}'^* + \delta\vec{s}'. \tag{11}$$

The linear approximation leads to,

$$\vec{\psi}'(\vec{s}'^* + \delta\vec{s}') \approx \vec{\psi}'(\vec{s}'^*) + \frac{d\vec{\psi}'}{d\vec{s}'}(\vec{s}'^*)\delta\vec{s}' = \vec{s}'^* + M'^*\delta\vec{s}' = \vec{s}'^* + \delta\vec{s}'. \tag{12}$$

Thus, the following expression is produced,

$$(M'^* - I')\delta\vec{s}' = 0, \tag{13}$$

where I' is a seven by seven identity matrix. From the structure of M' and the assumption of the turn in eccentricity,

$$(M'^* - I')\delta\vec{s}' = \begin{bmatrix} M^* - I & \frac{\partial\vec{\psi}}{\partial e}(\vec{s}^*) \\ 0_{1\times 6} & 0 \end{bmatrix} \begin{bmatrix} \delta\vec{s} \\ 0 \end{bmatrix} = 0, \tag{14}$$

where I is a six by six identity matrix. This equation reduces to,

$$(M^* - I)\delta\vec{s} = 0. \tag{15}$$

Thus, at the fold bifurcation, $\lambda = 1$ and $\delta\vec{s}$ always appear as eigenvalue and eigenvector for the six by six monodromy matrix, M. As the ER3BP is symplectic dynamics model, there exist a pair of unit eigenvalues at the fold bifurcation.

B. ER3BP POs: Family Tangent Direction and Proliferation of Broken Bifurcations

The proliferation of broken bifurcations for the ER3BP POs in illustrated in terms of the family tangent direction within the augmented space for $\vec{s}' \in \mathbb{R}^7$. Recall that the PO continuation process evolves with a fixed $T = \rho_E$ as evident from the grey plane in Fig. 8. Additionally, the continuation procedure assumes a constant mass parameter, μ, and results in one-parameter family evolution with respect to e. Within the fixed $T = \rho_E$ plane, although intersection with another family is potentially possible, leading to transcritical or pitchfork bifurcations, the intersection is often deformed into two broken branches within the ER3BP. For illustration, first note that the augmented monodromy matrix M' from Eq. (10) allows a maximum of one eigenvector that possesses a non-zero e component; this vector is denoted as $\vec{v}_e$. This vector coincides with the family tangent direction as appears within the fixed $T = \rho_E$ plane in Fig. 8 that is also apparent from

Eq. (12). Since the mapping function $\vec{\psi}'$ for the ER3BP PO fixed point is continuous, the eigenvectors of M' also evolve continously along family hodographs, including $\vec{v}_e$. Consider an example in Fig. 21(a), where the plane corresponds to the fixed $T = \rho_E$ plane on which the ER3BP POs evolve. Along the blue curve, Family A, the family tangent direction that coincides with $\vec{v}_{e,A}$ evolves continuosly. Due to this continuity of the family tangent direction, family intersections are expected to deform, resulting in two disconnected branches. Within Fig. 21(a), consider a second PO family colored in red (Family B). For both families, the family tangent directions, $\vec{v}_{e,A}$ and $\vec{v}_{e,B}$, evolve continuously. It is unexpected for the monodromy matrix, M', at the intersection, to produce two different eigenvectors. Thus, the families typically numerically evolve into two disconnected but continuous branches, as depicted in Fig. 21(b). Here, the two broken branches consist of the two families, but they are disconnected rather than producing a true intersection. Now, along each broken family curve, the family tangent direction $\vec{v}_e$ evolves continuously. Note that similar analysis applies to other one-parameter continuation schemes common for analyzing POs within periodically perturbed restricted body problems. While the true intersections in Fig. 21(a) may exist, they are expected to be sparse and subject to some symmetry properties [31], e.g., a period-doubling bifurcation within the $T = \rho_E$ plane. Demonstrating the existence of true intersections is beyond the scope of the current work; refer to Seydel [31] for numerical criteria for discerning true family intersections (transcritical, pitchfork) from fold bifurcations. In the context of the current investigation, it is sufficient to conclude that if another family exists nearby that originates from any nearby CR3BP structures, due to the one-parameter nature of the continuation scheme, the continuous family is likely to demonstrate broken bifurcations, as apparent in Fig. 21(b). For the ER3BP, and in the transition-challenging region, these broken bifurcations often take the form of fold bifurcations that lead the continuation process back to zero eccentricity, impeding the computation of ER3BP POs at the desired eccentricity value, $e = 0.055$.

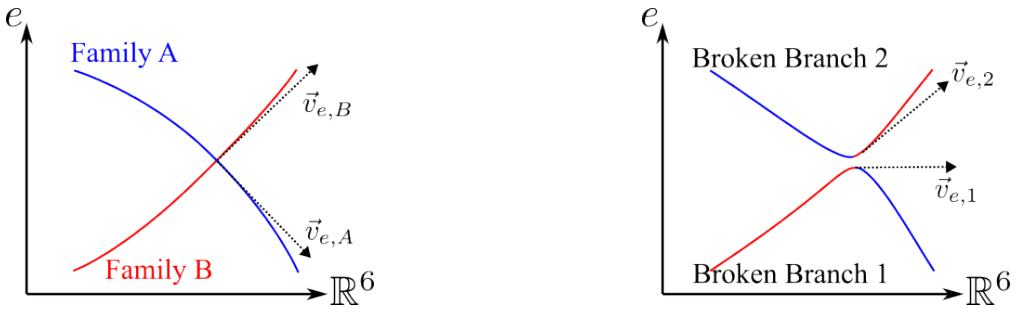

(a) True intersection **(b) Broken branches**

Fig. 21 Broken bifurcations and the family tangent eigenvectors

C. Numerical Continuation Scheme

The numerical formulation for targeting the POs and QPOs within the ER3BP is detailed. For the ER3BP PO associated with the $p:q$ resonant ratio, the total period is $2q\pi$. Leveraging the perpendicular crossing at the half period, the total propagation time is $q\pi$. Then, a multiple shooting scheme is employed where n segments are equally divided with respect to the independent variable between f_0 and $f_0 + q\pi$ within the ER3BP. The free variable vector (represented in a row vector format) for the targeter is constructed as,

$$\vec{X} = \begin{bmatrix} x_0 & z_0 & \dot{y}_0 & \vec{s}_2 & \dots & \vec{s}_n & e \end{bmatrix}, \tag{16}$$

where $x_0, z_0, \dot{y}_0$ correspond to the non-zero fixed point components at f_0. The subsequent states corresponding to the 2nd to n-th segments are denoted as $\vec{s}$ with a proper subscript. The last component for the vector $\vec{X}$ is the eccentricity associated with each PO. The constraint vector consists of,

$$\vec{F} = \begin{bmatrix} \vec{F}_c & \vec{F}_p \end{bmatrix}, \tag{17}$$

where the subscripts c and p correspond to the continuity between the segments and perpendicular crossing at the end of propagation from the last segment at $f_0 + q\pi$, respectively. A ER3BP PO results in a zero constraint vector. For the $p:q$, the number of segments is assigned as $n = 2p + 1$. Note that the lengths of $\vec{X}$ and $\vec{F}$ are $6n - 2$ and $6n - 3$, respectively;

thus, the Jacobian of $\vec{F}$ with respect to $\vec{X}$ allows one-dimensional null space. This null space vector is denoted as $\vec{V}_N$ with a length of $6n - 2$. Then, a pseudo-arclength continuation scheme enforces the following additional constraint.

$$F_N = \Delta\vec{X} \cdot \vec{V}_N - ds = 0, \tag{18}$$

where ΔX is the change in the free variable vector from the previously converged solution and ds is a user-defined nondimensional step size within the targeting process. The continuation process solves for $\vec{X}$ that satisfies Eqs. (17) and (18). Following discussions from Section IV.D, relevant factors for the continuation results include the number of segments (n) and the step size (ds). Larger n and smaller ds values result in a higher likelihood of locating additional fold bifurcations within the ER3BP PO continuation process as it results in denser effective step sizes with respect to e. While there exists no "correct" combination of values, the following set of parameters are utilized for the continuation scheme: $ds = 0.001$ and $n = 2p + 1$. For the QPO computation, refer to Park and Howell [11] for more details on the numerical formulation. A total of 51 discrete nodes are utilized for the invariant curve represetation, and $ds = 0.001$ is employed for the pseudo-arclength continuation.

References

[1] Zimovan-Spreen, E. M., Howell, K. C., and Davis, D. C., "Near rectilinear halo orbits and nearby higher-period dynamical structures: orbital stability and resonance properties," *Celestial Mechanics and Dynamical Astronomy*, Vol. 132, No. 5, 2020, pp. 1–25.

[2] Crusan, J. C., Smith, R. M., Craig, D. A., Caram, J. M., Guidi, J., Gates, M., Krezel, J. M., and Herrmann, N. B., "Deep space gateway concept: extending human presence into cislunar space," *2018 IEEE Aerospace Conference*, IEEE, 2018, pp. 1–10.

[3] McComas, D., Christian, E. R., Schwadron, N. A., Fox, N., Westlake, J., Allegrini, F., Baker, D., Biesecker, D., Bzowski, M., Clark, G., et al., "Interstellar Mapping and Acceleration Probe (IMAP): a new NASA mission," *Space science reviews*, Vol. 214, 2018, pp. 1–54.

[4] Clampin, M., "The James Webb Space Telescope (JWST)," *Advances in Space Research*, Vol. 41, No. 12, 2008, pp. 1983–1991.

[5] Dei Tos, D. A., and Topputo, F., "Trajectory refinement of three-body orbits in the real solar system model," *Advances in Space Research*, Vol. 59, No. 8, 2017, pp. 2117–2132.

[6] Davis, D. C., Phillips, S. M., Howell, K. C., Vutukuri, S., and McCarthy, B. P., "Stationkeeping and transfer trajectory design for spacecraft in cislunar space," *AAS/AIAA Astrodynamics Specialist Conference*, 2017, pp. 1–20.

[7] Dei Tos, D. A., and Topputo, F., "Trajectory refinement of three-body orbits in the real solar system model," *Advances in Space Research*, Vol. 59, No. 8, 2017, pp. 2117–2132. https://doi.org/10.1016/j.asr.2017.01.039, URL https://www.sciencedirect.com/science/article/pii/S0273117717300868.

[8] Oguri, K., Oshima, K., Campagnola, S., Kakihara, K., Ozaki, N., Baresi, N., Kawakatsu, Y., and Funase, R., "EQUULEUS trajectory design," *The Journal of the Astronautical Sciences*, Vol. 67, No. 3, 2020, pp. 950–976.

[9] Boudad, K., Howell, K. C., and Davis, D. C., "Analogs for Earth-Moon halo orbits and their evolving characteristics in higher-fidelity force models," *AIAA SCITECH 2022 Forum*, 2022.

[10] Park, B., and Howell, K. C., "Leveraging intermediate dynamical models for transitioning From the circular restricted three-body problem to an ephemeris model," *AAS/AIAA Astrodynamics Specialist Conference*, Charlotte, North Carolina, 2022.

[11] Park, B., and Howell, K. C., "Leveraging the elliptic restricted three-body problem for characterization of multi-year Earth-Moon L2 halos in an ephemeris model," *AAS/AIAA Astrodynamics Specialist Conference*, Big Sky, Montana, 2023.

[12] Gómez, G., Masdemont, J., and Mondelo, J., "Solar system models with a selected set of frequencies," *Astronomy & Astrophysics*, Vol. 390, No. 2, 2002, pp. 733–749.

[13] Lian, Y., Gómez, G., Masdemont, J. J., and Tang, G., "A note on the dynamics around the lagrange collinear points of the Earth-Moon system in a complete solar system model," *Celestial Mechanics and Dynamical Astronomy*, Vol. 115, 2013, pp. 185–211.

[14] Sanaga, R. R., and Howell, K. C., "Synodic resonant halo orbits in the Hill restricted four-body problem," *AAS/AIAA Astrodynamics Specialist Conference*, Austin, Texas, 2023.

[15] Sanaga, R. R., and Howell, K. C., "Analyzing the challenging region in the Earth-Moon L2 halo family through Hill restricted four-body problem dynamics," *AIAA SCITECH 2024 Forum*, 2024.

[16] Henry, D. B., Rosales, J. J., Brown, G. M., and Scheeres, D. J., "Quasi-periodic orbits around Earth-Moon L1 and L2 in the Hill restricted four-body problem," *AAS/AIAA Astrodynamics Specialist Conference*, Big Sky, Montana, 2023.

[17] Park, R. S., Folkner, W. M., Williams, J. G., and Boggs, D. H., "The JPL planetary and lunar ephemerides DE440 and DE441," *The Astronomical Journal*, Vol. 161, No. 3, 2021, p. 105.

[18] Hiday-Johnston, L., and Howell, K., "Transfers between libration-point orbits in the elliptic restricted problem," *Celestial Mechanics and Dynamical Astronomy*, Vol. 58, 1994, pp. 317–337.

[19] Wiesel, W. E., and Pohlen, D. J., "Canonical floquet theory," *Celestial Mechanics and Dynamical Astronomy*, Vol. 58, 1994, pp. 81–96.

[20] Williams, D., Howell, K. C., and Davis, D. C., "A comparison of station-keeping strategies for halo orbits," *AAS/AIAA Astrodynamics Specialist Conference*, Big Sky, Montana, 2023.

[21] Lujan, D., and Scheeres, D. J., "Earth–Moon L2 quasi-halo orbit family: characteristics and manifold applications," *Journal of Guidance, Control, and Dynamics*, Vol. 45, No. 11, 2022, pp. 2029–2045.

[22] Olikara, Z. P., "Computation of quasi-periodic tori and heteroclinic connections in astrodynamics using collocation techniques," Ph.D. Dissertation, University of Colorado at Boulder, 2016.

[23] Ferrari, F., and Lavagna, M., "Periodic motion around libration points in the elliptic restricted three-body problem," *Nonlinear Dynamics*, Vol. 93, No. 2, 2018, pp. 453–462.

[24] Campagnola, S., Lo, M., and Newton, P., "Subregions of motion and elliptic halo orbits in the elliptic restricted three-body problem," *AAS/AIAA Space Flight Mechanics Meeting*, Galveston, Texas, 2008.

[25] Peng, H., and Xu, S., "Stability of two groups of multi-revolution elliptic halo orbits in the elliptic restricted three-body problem," *Celestial Mechanics and Dynamical Astronomy*, Vol. 123, No. 3, 2015, pp. 279–303.

[26] Jorba, A., and Villanueva, J., "On the persistence of lower dimensional invariant tori under quasi-periodic perturbations," *Journal of Nonlinear Science*, Vol. 7, No. 5, 1997, pp. 427–473.

[27] Gómez, G., and Mondelo, J. M., "The dynamics around the collinear equilibrium points of the RTBP," *Physica D: Nonlinear Phenomena*, Vol. 157, No. 4, 2001, pp. 283–321.

[28] Olikara, Z. P., and Scheeres, D. J., "Numerical method for computing quasi-periodic orbits and their stability in the restricted three-body problem," *Advances in the Astronautical Sciences*, Vol. 145, No. 911-930, 2012, pp. 911–930.

[29] McCarthy, B. P., "Cislunar trajectory design methodologies incorporating quasi-periodic structures with applications," Ph.D. Dissertation, Purdue University, West Lafayette, Indiana, 2022.

[30] Olikara, Z. P., Gómez, G., and Masdemont, J. J., "A note on dynamics about the coherent Sun–Earth–Moon collinear libration points," *Astrodynamics Network AstroNet-II: The Final Conference*, Springer, 2016, pp. 183–192.

[31] Seydel, R., *Practical bifurcation and stability analysis*, Vol. 5, Springer Science & Business Media, 2009.

[32] Rosales, J. J., Jorba, A., and Jorba-Cuscó, M., "Families of halo-like invariant tori around L2 in the Earth-Moon bicircular Problem," *Celestial Mechanics and Dynamical Astronomy*, Vol. 133, No. 4, 2021, p. 16.

[33] Jorba-Cuscó, M., Farrés, A., and Jorba, À., "Two periodic models for the Earth-Moon system," *Frontiers in Applied Mathematics and Statistics*, Vol. 4, 32, 2018, pp. 1–14.

[34] Peng, H., Bai, X., and Xu, S., "Continuation of periodic orbits in the Sun-Mercury elliptic restricted three-body problem," *Communications in Nonlinear Science and Numerical Simulation*, Vol. 47, 2017, pp. 1–15.